Dynamic Bayesian network-based system-level evaluation on fatigue reliability of orthotropic steel decks

Heng, Junlin; Zheng, Kaifeng; Kaewunruen, Sakdirat; Zhu, Jin; Baniotopoulos, Charalampos

[Link to publication on Research at Birmingham portal](#)

1 **Dynamic Bayesian network-based system-level evaluation on fatigue**

2 **reliability of orthotropic steel decks**

3

4 **Junlin Heng[1,2], Kaifeng Zheng[1], Sakdirat Kaewunruen[2], Jin Zhu[1] and Charalampos**

5 **Baniotopoulos[2]**

6

7 [1] Department of Bridge Engineering, School of Civil Engineering, Southwest Jiaotong University,

8 Chengdu 610031, China

9 [2] Department of Civil Engineering, School of Engineering, University of Birmingham, Birmingham

10 B152TT, United Kingdom

11

12 **Abstract:** Fatigue fractures can be frequently observed in welded joints in orthotropic steel decks

13 (OSDs) after just a few decades of operation, which become the major deterioration mechanism

14 deterring the serviceability of OSDs. In this paper, a novel dynamic Bayesian network (DBN) model

15 has been established for the fatigue reliability analysis of OSDs at system-level. The exact inference

16 algorithm is applied in the DBN model with discrete variables. Special modifications have been made

17 on the existing algorithm to improve the computational efficiency in dealing with the deck system

18 which consists of a considerable number of joints. Using the DBN model, the fatigue reliability of

19 welded joints can be predicted and updated with the inspection and monitoring results at system-level.

20 At the same time, a framework is established for the system-level reliability considering the fatigue

21 fracture of rib-to-deck (RD) joints, the dominant cracking pattern affecting the serviceability of

22 OSDs. For illustration, a typical OSD bridge in China has been selected to carry out a case study. To

23 derive the stress spectrum required by the DBN model, the stochastic traffic model is employed, and

24 the influence-based Monte Carlo simulations have been carried out. As a result, the fatigue reliability

25 can be predicted at both component- and system-levels. Meanwhile, the observation of the traffic and

26 the inspection result has been fused into the DBN model to update the deteriorating state of the deck

27 system. Besides, the effect of enhancement and maintenance has been highlighted, including the

28 enhancement in fatigue strength at the construction stage, and the repair and traffic control during the

29 operation stage.

30 **Keywords:** orthotropic steel deck; fatigue reliability; system-level evaluation; dynamic Bayesian

31 network; stochastic traffic model.

32

33 **1. Introduction**

34   Orthotropic steel decks (OSDs) have been extensively used in modern steel bridges, because of

35 their advantages such as light self-weight, speedy construction and so on [1]. Under the continuous

36 loading of vehicles passing through the deck, fatigue damage will accumulate in welded joints of

37 OSDs and eventually lead to fatigue fractures, which is the critical deterioration mechanism of OSDs

38 [2]. Besides, due to the large number of welded joints adopted in OSDs, the fatigue-induced

39 deterioration has become the major cause degrading the serviceability of OSDs.

40   Generally, the fatigue damage is highly stochastic, due to the significant uncertainties in fatigue

41 strength (resistance) and vehicle loads (loading effects). Thus, if fatigue evaluation is performed in a

42 deterministic manner, it may deviate from the stochastic nature and lead to inaccurate results [3]. A

43 feasible way is to evaluate fatigue performance in a probabilistic way, i.e., fatigue reliability analysis

44 [4]. In recent years, extensive efforts have been conducted by many researchers on the aspect. Kwon

45 and Frangopol [3] proposed a method for fatigue reliability assessment of steel bridges incorporating

46 the field-measured stress spectrum, in which fatigue strength and stress ranges were treated as random

47 variables. Case studies were performed for the critical details in two bridges, and the remaining life

48 was estimated by setting target reliability. Guo et al. [5] proposed a probabilistic traffic model through

49 the statistics on the measured data. Finite element model was established to transfer the traffic model

50 into the stress ranges of critical details, which were then used in the reliability analysis. Lu et al. [6]

51 employed the machine learning method to derive the stress spectrum using the stochastic traffic

52 model. Monte Carlo simulations were then applied to calculate the fatigue reliability of critical details.

53 Zhou et al. [7] conducted statistics on the vehicle loads collecting from four bridges in different

54 regions of France. The lateral position of vehicles was measured and analysed. Based on that,

55 probabilistic traffic model was established, and stress spectra were derived.

2

56   As stated above, these studies mainly focused on the fatigue reliability analysis at component-

57   level, in which the number of details has been ignored. However, this may lead to inaccurate results,

58   since the deck system consists of various details. For instance, fatigue fractures are more likely to be

59   observed in a structural system consisting of 1,000 fatigue-critical details than the one with only one

60   fatigue-critical detail. Currently, few publications could be found on the fatigue reliability of OSDs at

61   the system-level. Maljaars and Vrouwenvelder [8] established a probabilistic fatigue damage model

62   for the critical detail in OSDs, using the presumed stress spectra. The multiple presences of similar

63   details were considered by treating the OSD as a pure series system consisting of components with the

64   same failure rate. The results suggested that the reliability of 100 similar details was significantly

65   lower than that of a single detail.

66   Usually, the crude Monte Carlo method is used in the reliability analysis due to its concision and

67   flexibility [6][9]. However, its computational efforts would gradually become intractable when the

68   failure rate reaches a small value. The problem can be ameliorated to some extent by using the

69   advanced Monte Carlo methods such as importance sampling, directional sampling, and adaptive

70   sampling. However, these methods also have their limitations and sometimes become infeasible [10].

71   Alternatively, approximation methods such as first/second order reliability methods (FORM/SORM)

72   can be employed [11]. Nonetheless, when the limit state function is highly nonlinear, the accuracy and

73   computational efficiency of these methods will significantly decrease [12]. Also, the above methods

74   are unable to perform reliability updating and information fusion, which further restrict their

75   applications. Even if these tasks could be partly performed by Monte Carlo simulations with

76   conditional probability, the computational cost would become incredibly high [8].

77   Recently, to overcome the above difficulties, the Bayesian network (BN) methodology has been

78   proposed as an effective framework for reliability assessment at system-level. The BN is particularly

79   suitable for system reliability assessment because it enables the uncertainty propagation and updating

80   through nodes/components in the network that allows the transformation of information from the

81   system-level to component-level. Straub [13] proposed a general dynamic Bayesian network (DBN)

82   framework for the reliability analysis of deterioration processes. The study suggested that the

83   computational efficiency and robustness in prediction and updating made the DBN particularly

84   suitable for the reliability analysis of deterioration processes. In the next, Luque and Straub [14]

85   extended the general framework to the system-level reliability analysis of deteriorating systems. Zhu

86   et al. [15] established a DBN model for the fatigue assessment of a single detail in OSDs. The particle

87   filer-based approximation inference algorithm was used, and the result showed that the DBN model is

88   capable to predict and calibrate the fatigue damage of OSDs.

89   The objective of this paper is to evaluate the fatigue reliability of orthotropic steel decks (OSDs)

90   at system-level. A DBN model has been established for the system-level fatigue reliability of OSDs,

91   aimed at the prediction, information-based fusion and evidence-based update. In the model, the exact

92   inference algorithm has been employed with discrete variables. Special modifications have been made

93   on the existing algorithm to improve the computational efficiency in dealing with the large-scale deck

94   system consisting of massive fatigue-critical details. Meanwhile, a framework of system-level

95   reliability has been established for OSDs basing on the serviceability. In the DBN model, the fatigue

96   action is considered by the combination of random traffic volume and deterministic stress spectrum.

97   In deriving stress spectra, the stochastic traffic model has been employed incorporating with the

98   multi-scale finite element model. Through employing the influence-surface technology, sampling-

99   based analysis has been performed with a large sample-size to obtain comprehensive stress spectra.

100   Based on the established method, a typical OSD bridge in China has been selected to carry out a

101   case study. At first, the fatigue reliability of the deck is predicted without monitoring results, and the

102   effect of strength enhancement has been analysed. Meanwhile, the fusion of observed traffic

103   information has also been illustrated with the model. After that, two types of inspection results have

104   been considered to update the model, i.e., the non-detection and the detection of fatigue cracks.

105   Finally, the effect of treatment approaches on the deteriorated deck system has been investigated,

106   including the maintenance and traffic control.

107   **2.   Development of DBN for OSDs at system-level**

108   **2.1 Capability of DBN in modelling the deteriorating process**

109   The dynamic Bayesian network (DBN) is a powerful probabilistic tool originated in computer

110   science [16], which is naturally suitable for modelling the deterioration process in structures. Fig. 1

shows a simple model of DBN, in which X stands for the variables in the state space, such as material

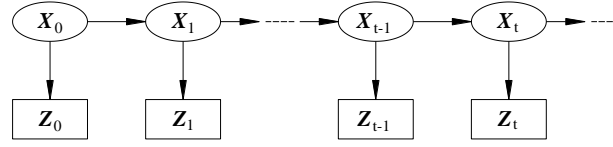properties and loading effects; Z stands for the evidence of current states, e.g. damage state.

Fig. 1. Constructed mesh of sample model.

With the DBN model, several probabilistic tasks could be conducted using various algorithms

[17]. Among them, the following three tasks are commonly involved in the deterioration analysis:

(1) prediction: the task is to predict the possible state of the system in the future time slice t, as

shown in Eq. 1.

$$\Pr(\boldsymbol{X}_t) = O(\Pr(\boldsymbol{X}_{t-1})) = \cdots = O^t(\Pr(\boldsymbol{X}_0)) \#(1)$$

where the symbol O stands for the operation function of state transition between time slices; the

symbol O^t indicates the state transition is repeated for t times.

(2) information-based fusion: the task is to fuse the new information about the state space (e.g.

the new physical model or probabilistic model) into the DBN model at the specific time slice, based

on the previous state, as shown in Eq. 2.

$$\Pr(\boldsymbol{X}_{t+1}) = O'(\Pr(\boldsymbol{X}_t)) \#(2)$$

Where the symbol O' represents the state transition using the fused model.

(3) evidence-based updating: the task is to update the probability distribution of the state space

with the evidence, as shown in Eq. 3.

$$\Pr(\boldsymbol{X}_t|\boldsymbol{Z}_t) \propto \Pr(\boldsymbol{X}_t) * \Pr(\boldsymbol{Z}_t|\boldsymbol{X}_t) \#(3)$$

Where symbol $\propto$ stands for similarity between the two ends of the equation, and the exact value could

be solved by normalization; $\Pr(\boldsymbol{Z}_t|\boldsymbol{X}_t)$ is the likelihood factor representing the possibility of evidence

$\boldsymbol{Z}_t$ under the assumed state $\boldsymbol{X}_t$.

By performing the Eq. 3 recursively, the updated probability distribution of state space could be

obtained basing on evidence over the past time slices from 0 to t, i.e., $\Pr(\boldsymbol{X}_t|\boldsymbol{Z}_{0:t})$. In addition,

performing the Eq. 1 on this basis, the prediction at the future time slice T could be made with the

updated model, i.e., $\Pr(\boldsymbol{X}_T|\boldsymbol{Z}_{0:t})$, where $t<T$.

134   **2.2 Construction of the DBN model for OSDs**

135   *2.2.1 Deterioration model of fatigue damage*

136   Several approaches are available for fatigue assessment of welded joints, which could be

137   classified into two categories: damage factor-based stress-life (S-N) approach and crack size-based

138   fracture mechanics (FM) approach [18][19]. The FM approach is close to the cracking nature and able

139   to consider the sequence effect of loads. However, high computational efforts are usually required in

140   FM approaches, which makes it somehow intractable for the system-level reliability problem.

141   Meanwhile, with the well-established database, the S-N approach could also generate satisfactory

142   results in engineering problems. Thus, an advanced S-N approach, the hot spot stress approach, has

143   been applied [20]. The two-stage model proposed by Eurocode 3 [21] has been applied, and the

144   fatigue deterioration model is derived, as shown in Eqs. 4a and b,

$$D_{i,t} = \begin{cases} \left(\dfrac{\Delta\sigma_i}{\Delta\sigma_D}\right)^{m_1} \cdot \dfrac{n_{i,t}}{N_D}, & \Delta\sigma_i \leq \Delta\sigma_D \\[2ex] \left(\dfrac{\Delta\sigma_i}{\Delta\sigma_C}\right)^{m_2} \cdot \dfrac{n_{i,t}}{N_C}, & \Delta\sigma_i > \Delta\sigma_D \end{cases} \#(4a)$$

$$D_{sum}(t) = \sum_t \sum_i D_{i,t} \#(4b)$$

145   where $D_{i,t}$ is the damage increment induced by the stress block $\Delta\sigma_i$ at the time slice t; $n_{i,t}$ is the

146   corresponding number of cycles; $\Delta\sigma_C$ and $\Delta\sigma_D$ are respectively fatigue strength at 2 million cycles and

147   5 million cycles; m_1 and m_2 are the power indexes for the stage 1 and the stage 2, which equal to 3

148   and 5, respectively; N_C and N_D equal to 2 million and 5 million, respectively; $D_{sum}(t)$ is the total

149   damage factor at the time slice t.

150   In the model, the stress block $\Delta\sigma_i$ and corresponding cycle $n_{i,t}$ represent the vehicle-induced

151   stress ranges, which will be discussed later in the derivation of stress spectra. The fatigue strength

152   parameters $\Delta\sigma_C$ and $\Delta\sigma_D$ can be determined by the strength model in the design code [21] or the

153   numerical analysis [22]. In the S-N approach, failure is achieved when the damage factor reaches a

154   specific value. To this end, the limit state function could be established, as shown in Eq. 5,

$$g(D,t) = \Delta - D_{sum}(t) \#(5)$$

155   where Δ is the accumulation factor and assumed as 1.0 in this study.

156   *2.2.2 Variables considered in the DBN model*

157   In the deterioration model, the uncertainties originate from both the resistance (i.e. the fatigue

158   strength) and action (i.e. the stress ranges induced by vehicle loads). The fatigue strength is treated as

159   a time-invariant random variable R. In the case of fatigue action, a high traffic volume is generally

160   expected over the time slice (e.g. half million per year per lane). Due to Borel's law of large numbers

161   [23], the proportion of each stress range approximates to the actual probability with the increase in

162   traffic volume. On this basis, the fatigue action is represented by the deterministic stress spectrum and

163   the random traffic volume. Meanwhile, the stress spectrum is solved under the stochastic model with a

164   large sample-size to reflect the diversity of stress ranges, which will be illustrated in detail later. The

165   traffic volume is represented by the average daily traffic (ADT), derived from the traffic model in

166   codes or by observation.

167   *2.2.3 Hyper parameter-based correlation*

168   The welded joints in OSDs are usually fabricated by the steel in the same grade (or even the

169   same production batch) by the same manufacturer, using similar welding technology and quality

170   assurance. Meanwhile, those joints will experience the same traffic during the operation. Due to the

171   above factors, it will result in the correlation between state variables of joints. Two types of

172   correlations have been considered: (1) the correlation in fatigue strength; (2) the correlation in ADT.

173   To simulate the correlations, the hierarchical model with hyper-parameters has been applied [14]. The

174   variables are considered as equally correlated, which have the mutual correlation coefficient ρ_X and

175   identical marginal distribution. To interrelate the variables statistically, an uncertain common hyper-

176   parameter α has been introduced, which follows the standard normal distribution. Basing on that, the

177   cumulative distribution function (CDF) of each variable is assumed to be conditional on the hyper-

178   parameter, as shown in Eq. 6,

$$F_{X|\alpha}(x) = \Phi\left(\frac{\Phi^{-1}[F_X(x)] - \sqrt{\rho_U} * \alpha}{\sqrt{1 - \rho_U}}\right) \#(6)$$

179   where Φ and Φ^{-1} are respectively the CDF and inverse CDF of the standard normal distribution;

180    $F_X(x)$ is the marginal CDF of the variables in the correlated set; ρ_U is the correlation coefficient in the

181   standard normal space.

182   The coefficient ρ_U could be determined from the marginal CDF $F_X(x)$ and the original

183   coefficient ρ_X, as shown in the literature [24]. In the case of ADT, the condition $\rho_X = 1$ could be

184   assumed, i.e., perfectly correlated.

185   *2.2.4 Construction of the DBN for OSDs*

186   Basing on the above analysis, the DBN model has been constructed for the system-level fatigue
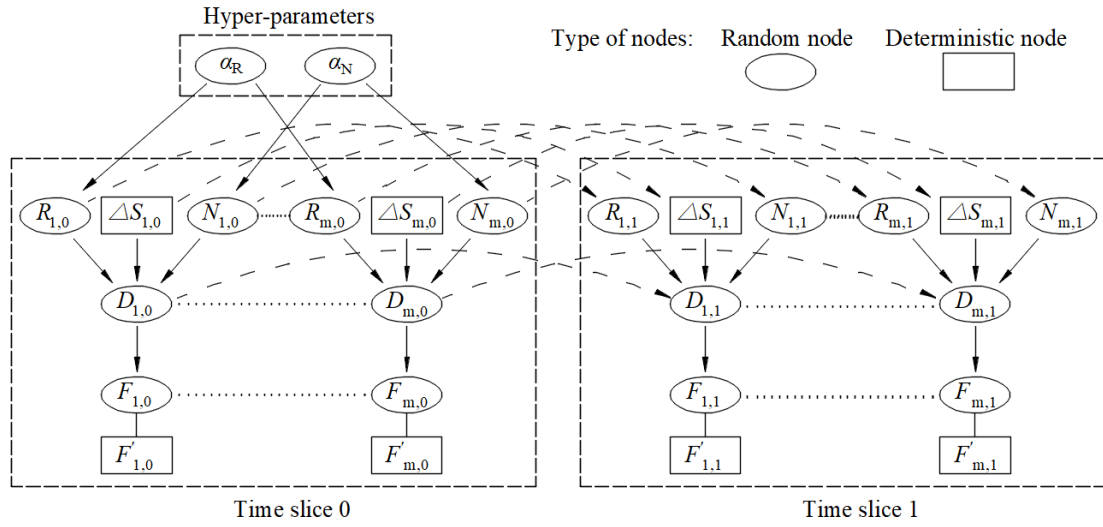
187   reliability of OSDs, as shown in Fig. 2.

188

Fig. 2. DBN model for fatigue damage of joints in OSDs.

189

190

191   Two types of nodes have been employed in modelling: (1) the random node with an elliptical

192   box; (2) the deterministic node with a rectangular box. The notations of nodes are summarised in

193   Table 1. Meanwhile, the solid arrow represents the inner-relation between different nodes in the same

194   time slice, while the dashed arrow stands for the inter-relation between the same nodes in two

195   adjacent time slices.

196

Table 1 Notations in the DBN model

Notation	Type	Description
α_R	Random	Hyper-parameter of the fatigue strength
α_N	Random	Hyper-parameter of the ADT
$R_{i,t}$	Random	Fatigue strength of the ith joint at time t
$\Delta S_{i,t}$	Deterministic	Stress spectrum of the ith joint at time t
$N_{i,t}$	Random	The ADT of the ith joint at time t
$D_{i,t}$	Random	Damage factor of the ith joint at time t
$F_{i,t}$	Random	Failure state of the ith joint at time t
$F'_{i,t}$	Deterministic	Evidence of failure state of the ith joint

197

2.3 Computation algorithm of the proposed DBN model

2.3.1 Discrete DBN with exact inference

Generally, DBNs could be classified into two categories by the type of nodes: (1) continuous DBN consisting of continuous variables; (2) discrete DBN consisting of discrete variables. Meanwhile, various algorithms have been proposed for the two types of DBNs [25]. Obviously, the continuous DBN is perfectly suitable for fatigue deterioration since most of the variables are naturally continuous. However, the inference algorithms developed for continuous DBNs are generally sampling-based [17], in which the computational efficiency decreases rapidly with the increase in the number of nodes and the decrease in the probability of interest (e.g. the probability of failure). The OSD system consists of a considerable number of joints with a low failure rate, for which the continuous DBN is not feasible. Alternatively, the discrete DBN with the more efficient exact inference has been applied in this study, whose feasibility has already been proved in literature [14][26].

2.3.2 Likelihood-based parallel updating method

In the discrete DBN, the frontier algorithm is extensively used due to its concision and flexibility [16]. In the method, the state transition is conducted through sweeping the joint probability, called as the frontier, across the network. When evidence is available, e.g. the observation of cracks in structural members, the DBN model can be automatically updated as shown in Eq. 3. A notable feature of the method is that the joint probability of the entire state space will be constructed during the transition, which makes it computationally intractable in dealing with the large-scale system. Take a system consisting of m components as an example. If each component has N possible states, the computational complexity could be regarded as $O(N)$. Moreover, the system will approximately have a complexity of $O(N^m)$, which will increase exponentially with the number of components m. Thus, the frontier algorithm has been modified according to the features of the established DBN.

Since the joint probabilities of the components are connected through the shared hyper-parameters only, the original frontier algorithm could be adapted to a parallel-solving way. To achieve that, the concept of the component-level frontier is introduced: the frontier containing only the state of one component and the shared hyper-parameters. At the beginning of each solving step, these

frontiers are parallelly transferred. During the transition, the component-level likelihood could be solved for the hyper-parameters, based on the evidence of the ith component, as shown in Eq. 7,

$$L_{i,t} = \Pr\left(F'_{i,t}\middle|\boldsymbol{\alpha}\right) = \frac{\Pr\left(\boldsymbol{\alpha}\middle|F'_{i,t}\right)}{\Pr(\boldsymbol{\alpha})} \#(7)$$

where $L_{i,t}$ stands for the component-level likelihood of the ith component; $\boldsymbol{\alpha}$ is the vector of hyper-parameters, which are (α_R, α_N) in this study; $F'_{i,t}$ denotes the evidence of the failure state of the ith component.

After that, the component-level frontiers could be parallelly updated by the evidence of other components, as shown in Eq. 8,

$$\Pr\left(\boldsymbol{X}, \boldsymbol{\alpha}\middle|F'_{1:m,t}\right) \propto \prod_{\{1:m\}/\{i\}} L_{i,t} * \Pr\left(\boldsymbol{X}, \boldsymbol{\alpha}\middle|F'_{i,t}\right) \#(8)$$

where $\boldsymbol{X}$ is the vector of state space, including the nodes $R_{i,t}, N_{i,t}, D_{i,t}, F_{i,t}$ in this study; m is the number of components in the system; $\{1:m\}/\{i\}$ means the assemble from 1 to m except i.

3. System-level framework for fatigue reliability of OSDs

3.1 Case study: a typical OSD bridge in China

Among all the welded joints, fatigue fracture is frequently observed in the rib-to-deck (RD) joints. Two primary reasons could be attributed to: (1) the wheel loads directly acting on the deck will cause high-level local stresses in the joints; (2) the RD joint accounts for the largest proportion of welded joints in OSDs. Meanwhile, the fatigue cracking in RD joints may lead to severe consequences: the serviceability of the bridge would be directly affected, and it may even pose a threat to the safety of passing vehicles. From the perspective of serviceability, the fatigue cracking of RD joints could be regarded as the dominated cracking pattern of OSDs [27]. To this end, the RD joint is focused when establishing the framework of system-level fatigue reliability for OSDs. For illustration, a typical OSD bridge in China has been selected to carry out a case study, which is called as the prototype bridge, as shown in Fig. 3.

The prototype bridge has a total length of 158 m, consisting of a middle-span of 68 m and two side-spans of 45 m. The deck system of the bridge is divided into 112 segments, carrying three lanes

with 15 U-ribs. The details about the bridge are shown in Table 2. For illustration, the U-ribs are

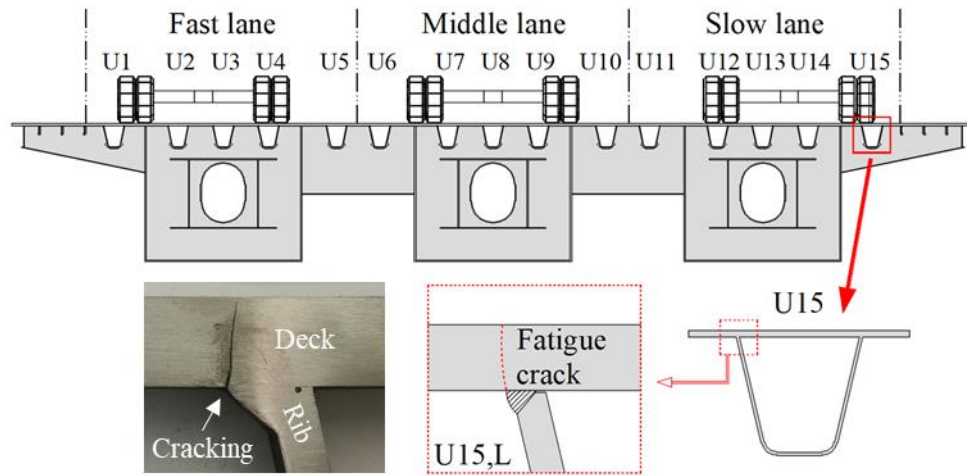named as U1 ~ U15 with a footnote of 'L' or 'R' representing the left or right joint of the U-rib.

Fig. 3. Fatigue cracking pattern of the prototype bridge

Table 2 Basic parameters of the object bridge

Parameter		Description
Span arrangement		45 m + 68 m + 45 m
Lane configuration (from left to right)		Fast + Middle + Slow
Number of segments		112
Number of U-ribs in a segment		15
Thickness (mm)	Deck	16
	U-ribs	8
	Floor beam	12
Welding profile of RD joints		One-sided with 80% penetration rate

3.2 Development of the system-level framework

As aforementioned, the deck system consists of considerable RD joints. Thus, the state of all the

joints should be considered in describing the state of the system. However, the combination of

component states will become incredibly large, which makes the system-level analysis almost

impossible. Take a deck system consisting of N joints as an example. If each joint has two states (i.e.,

0 = not failure, 1 = failure), the deck system will have 2^N possible states, which is an intractable NP-

hard problem. Thus, it is essential to find out a more efficient way to represent the fatigue

deterioration state of the deck system. Two unique features of the deck system could be utilized: (1)

the deck is able to work with the presence of limited cracks due to the high redundancy [28]; (2)

fatigue cracking of RD joints is more of a serviceability problem rather than the safety issue, which

will not cause catastrophic structural failures directly. Thus, the conception of Daniel system has been

266 applied, in which the number of failed components in the system is employed to represent the state of

267 the system [29].

268   Generally, the deck system is divided into a series of segments by the floor beams. Thus, the

269 deck system can be idealised as a multi-level framework, as shown in Fig. 4. By assuming that

270 cracking in any joint will cause misfunction of the entire segment, the segment is modelled as a series

271 system consisting of several RD joints. As a result, the failure of segments is achieved after the failure

272 of any RD joint. Meanwhile, the cracking in one segment will have little influence on other segments

273 as the deck system is highly redundant [28][30]. On this basis, the deck system is modelled as a

274 parallel system of the segments, whose deterioration state is represented by the number of failed
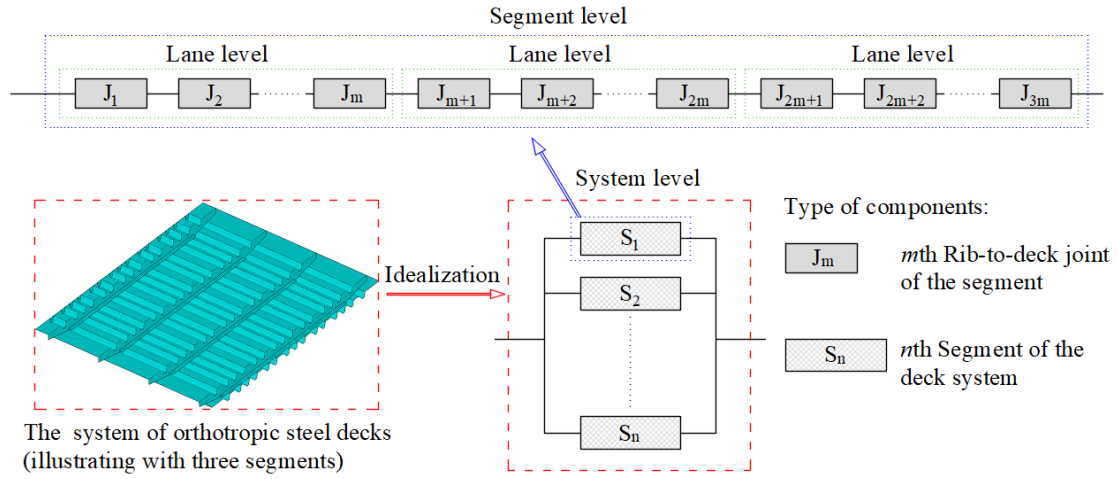
275 segments.

277 **Fig. 4.** Framework of the system-level reliability

278   Basing on the limit state function shown in Eq. 5, the probability of failure of the mth joint could

279 be expressed as Eq. 9,

$$\Pr\big[F_{J,m}(t) = 1\big] = \Pr\big[g_{J,m}(D,t) \leq 0\big] \#(9)$$

280 where the subscript 'J' is abbreviated for joint while the subscript 'm' is the sequence number of the

281 joint; $F_{J,m}(t)$ stands for the fatigue damage state of the mth joint in the segment at time t, with the

282 value of 1 or 0 representing failure or not failure respectively; $g_{J,m}(D,t)$ is the limit state function of

283 the mth joint at time t.

284   After that, the failure probability of the segments could be derived under the assumption of the

285 series system, as shown in Eq. 10,

$$\Pr[F_{seg,n}(t) = 1] = \Pr\left[\bigcup_m F_{J,m}(t) = 1\right] = 1 - \prod_m \left(1 - \Pr[F_{J,m}(t) = 1]\right) \quad \#(10)$$

where $F_{seg,n}$ stands for the failure state of the *n*th segment, in which value 0 or 1 stands for not failure and failure respectively.

Above all, the failure probability of the system is defined as the probability that the number of failed segments is no less than a specific value, as shown in Eq. 11,

$$P_{f,sys}(t, k) = \Pr[N_{f,seg}(t) \geq k] = \Pr\left[\sum_n F_{seg,n}(t) \geq k\right] \quad \#(11)$$

where $N_{f,seg}$ stands for the number of failed segments; k is the number of expected failed segments.

Correspondingly, the system-level reliability also reflects the probability that the number of failed segments is no more than k. It is worth stating that the value k should be determined based on the expectation on the serviceability of bridges. It also associates with the decision-making process of the inspection and maintenance plan [31], which is outside the scope of this study. Alternatively, an empirical failure percentage *k/n* of 30% has been used in this study, after consulting both the senior structural engineers, manufacturers and bridge management authorities.

4. Stress spectrum analysis using stochastic traffic model

4.1 Stochastic traffic model

4.1.1 Framework of the stochastic traffic model

As stated before, the stress spectrum is crucial information in the fatigue analysis. With the help of advanced monitoring systems, the stress spectrum could be established directly by monitoring [3][32]. However, because of the limitation on budget and feasibility, the monitoring system could not be extensively applied. Alternatively, the structural analysis with traffic models could be employed. Under this approach, the accuracy of spectra dependents on the rationality of the applied traffic model. In the code-specific design, the stress spectrum is represented by the effective stress range solved with the deterministic truck model [21][33]. Meanwhile, a series of correction factors are used to consider the uncertainties in traffic [34][35][36]. Obviously, this deviates from the stochastic nature of the traffic loads and may lead to inaccurate results [3] [37].

309　　　To overcome the problem, the stochastic traffic model has been applied to derive stress spectra.

310　　The traffic could be considered as the assembly of random vehicles passing through the bridge in

311　　various lateral positions stochastically. On this basis, the framework of the stochastic traffic model

312　　could be established, including both the model of vehicles and their lateral distribution. Since the

313　　stress of RD joints is directly determined by vehicles [1], the model is parametrised in detail with axle

314　　numbers, axle spacing, wheel tracks, axle weights, and footprints. Meanwhile, the lateral distribution

315　　of vehicles is described by lane occupancy rates and the in-lane position. Besides, the traffic volume

316　　is described by the average daily traffic (ADT). The parameters in the framework are summarised in

317　　Table 3. The distribution of parameters could be determined after either codes and specifications, or

318　　field observation, which will be discussed later.

319

Table 3 Parameters in the framework of the stochastic traffic model

Type	Parameter	Description
Vehicle property	Axle number	The number of axles in a vehicle
	Axle spacing	The distance between the center of axles
	Wheel track	The distance between wheels in the same axle
	Axle weight	The weight of each axle in a vehicle
	Footprint	The contact area of wheels on the deck
Lateral position	Occupancy rate	The distribution of the vehicle in different lanes
	In-lane position	The lateral position of the vehicle within a lane
Traffic volume	ADT	The number by averaging annual traffic to one day

320　*4.1.2 Data source of the stochastic traffic model*

321　　　After the innovative framework of stochastic traffic is established, the parameters could be

322　　determined from two main sources: (1) the existing data in publications such as codes and

323　　specifications; (2) direct measurements by monitoring systems. Obviously, the data from the site-

324　　specific measurements could reflect the real traffic on the specific bridge more accurately, which

325　　could in turn narrow down the uncertainties. However, this type of data is unavailable before the

326　　implementation of monitoring systems. Besides that, the availability of data is also associated with the

327　　number of sensors in the monitoring system. In this case, the capability of DBNs in information-based

328　　fusion could be utilised. At first, the default traffic model could be established based on existing data,

329　　which is subsequently used to derive the original stress spectra. Whenever more data are available, the

330　　traffic model could be easily updated to obtain the new stress spectra. Then the new spectra could be

331　　fused into the DBN model to evaluate time-dependent fatigue reliability.

332   In the study, the default model is first established with the standard truck model defined in

333   Eurocode (EC) 1 [34], as shown in Fig. 5. In the model, a deterministic 4-axle truck is used as the

334   representative of vehicles, in which the impact factor has been already included. Meanwhile, EC1

335   suggests that in the lanes predominantly used by cars (i.e. the fast lane and middle lane), the truck

336   traffic number could be considered as 10% of the number in the slow lane. On this basis, the

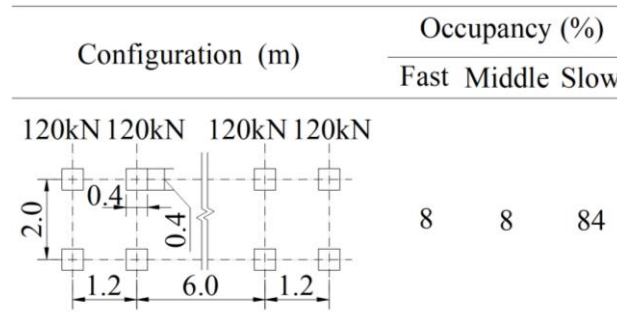337   occupancy rate of the standard truck could be determined, which is also included in Fig. 5.

338

339   **Fig. 5.** Standard truck model proposed in Eurocode 1

340   As aforementioned, the lateral position associates with both the occupancy rate and the in-lane

341   position. In the study, the distribution proposed in EC1 is used for the in-lane lateral position. To

342   facilitate its application in numerical simulation, the discrete distribution has been transformed into a
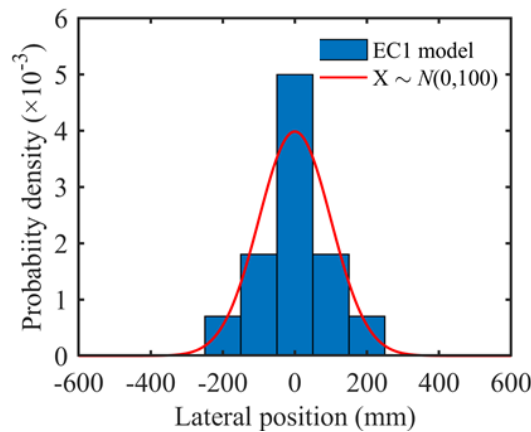
343   normal distribution, as shown in Fig. 6.

344

345   **Fig. 6.** Distribution of the in-lane lateral position

346   When the new traffic model is available, the new stress spectra can be derived and fused into the

347   DBN model. For illustration purpose, an observed traffic model measured in another typical OSD

348   bridge in China has been considered. Table 4 shows some basic information about the model, while

349   details could be found in the article [38].

350

**Table 4** Vehicle types and occupancy in the observed model

Type	Description	Lane occupancy (%)		
		Fast	Middle	Slow
1	Two-axle cars	41.23	25.74	9.70
2	Three-axle trucks (I)	0.03	0.26	0.36
3	Three-axle trucks (II)	0.10	0.87	0.60
4	Four-axle trucks	0.04	0.67	0.92
5	Five-axle trucks	0.06	1.17	1.31
6	Six-axle trucks	0.57	7.94	8.43

351   Since the in-lane position was not provided in the observed model, it keeps the same with the one

352   depicted in Fig. 6. Meanwhile, the footprints of tire have been adjusted as per the Chinese code [39],

353   which are respectively 0.3×0.2 m for front axles and 0.6×0.2 m for rear axles. Besides, an impactor

354   factor of 1.15 is considered [33].

355   **4.2 Influence surface-based stress spectrum analysis**

356   *4.2.1 Multi-scale finite element model*

357   To transfer the traffic model into stress spectra, a multi-scale finite element (FE) model has been

358   established for the prototype bridge in ANSYS software [40], as shown in Fig. 7.

359
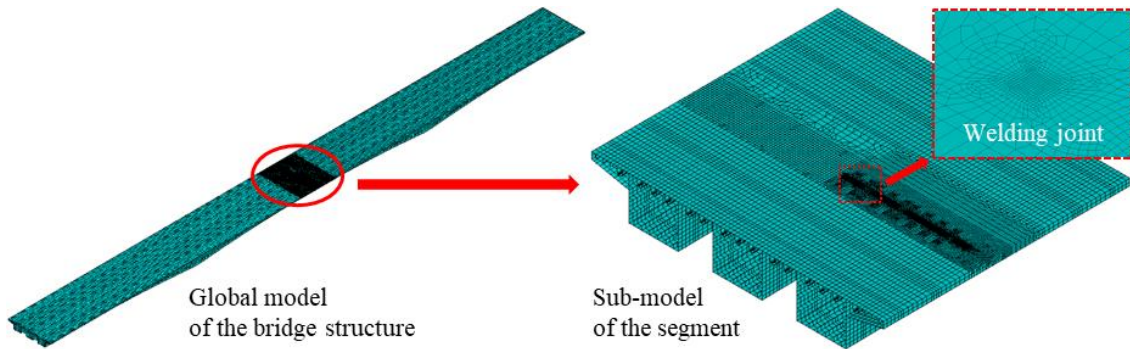
360   **Fig. 7.** Multi-scale finite element model of the prototype bridge

361   Generally, fatigue cracking of RD joints is mainly induced by the transverse stress, on which the

362   longitudinal location of segments has little influence [1]. Since all the segments of the OSD have

363   identical geometry, the joints in the same lateral position of different segments will have similar stress

364   spectra. Thus, the segment in the midspan is selected as the representative to derive the spectra. The

365   FE model consists of three parts in different meshing sizes: (1) the global model of the bridge

366   structure, simulating the boundary condition of the selected segment; (2) the sub-model of the selected

367   segment, served as a link between the relatively coarse global model and the highly refined detail

368   model; (3) the detail model of RD joints, in which the minimum element size is gradually refined to 1

16

369   mm near the joints. The 3-dimensional shell element is used, and only half of the joints are refined

370   with the detail model due to the symmetry of the deck.

371   *4.2.2 Influence surface-based calculation*

372   Based on the established model, Monte Carlo (MC) simulations are employed to derive the stress

373   spectrum from the traffic model. To obtain the comprehensive spectra, a large sample-size, e.g. 10^5, is

374   required even if stratified sampling is used. Besides, the computational cost is relatively high to derive

375   the vehicle-induced stress history from the FE model directly. For instance, it may require 100 or

376   more solving steps to calculate the stress history induced by just one vehicle. Thus, it becomes

377   computationally intractable with the large sample size. Thus, the influence-surface technology has

378   been used. Through a series of FE analysis, the influence-surface of RD joints could be established.

379   Fig. 8 shows the result of the joint $U12_L$, which is unitized after the maximum response for better

380   illustration. In the next, the stress history could be solved by direct superposition of the influence-

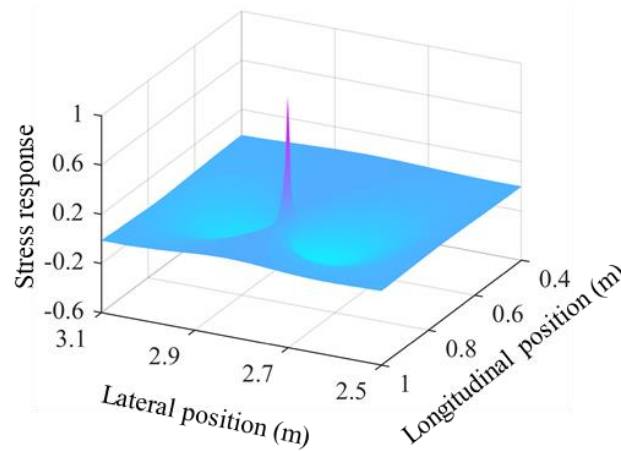381   surface according to the configuration of vehicles, which is much more computationally efficient.

382

383   **Fig. 8.** Influence-surface of the rib-to-deck joint $U12_L$

384   The calculation process is shown in Fig. 9. At first, a large-size database of vehicles, i.e. 10^7 in

385   this study, can be established through sampling according to the stochastic traffic model. FE analysis

386   is then performed to generate the influence-surface of each joint. After that, a Monte Carlo-based

387   program has been coded in MATLAB [41] to solve the stress history from the traffic data using the

388   influence-surface. Finally, the database of stress history is transformed into stress spectra using cycle-

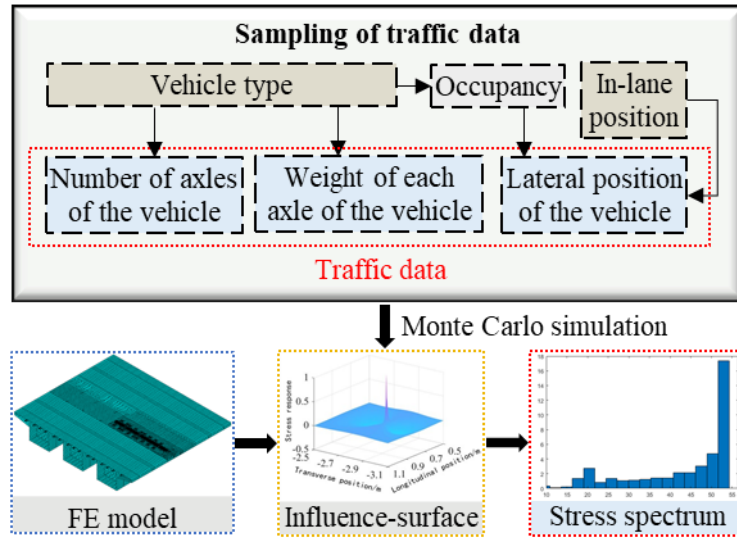389   counting methods such as the rain flow approach [42].

390

391 **Fig. 9.** Calculation process of the stress spectrum

392 The stress spectrum of the RD joint U12L in the slow lane has been shown in Figs. 10a and b,

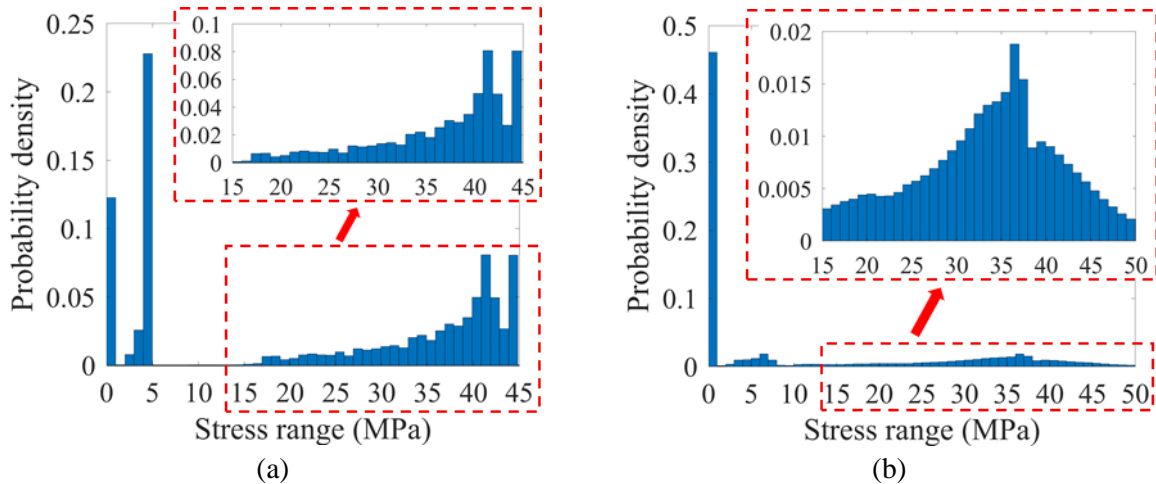393 which are respectively solved under the standard truck model and the observed model.

(a)   (b)

394 **Fig. 10.** Stress spectra of the joint U12$_L$: (a) standard truck model; (2) observed model.

395 For better demonstration, the stress ranges with a small possibility are truncated in Fig. 10b. The

396 result shows that under both models, the low-level stress ranges (less than 15 MPa) account for the

397 largest proportion. Meanwhile, the observed model could generate a more even and continuous

398 spectrum, compared with that induced by the standard truck model. This is because the standard truck

399 model only considers the lateral position as the random variable, while the observed truck model

400 includes many other random variables such as the vehicle type, axle weight, etc. Obviously, the

401 observed model can provide an in-depth consideration of the randomness in the traffic at the site.

18

402 **5. Reliability analysis using the established DBN model**

403 **5.1 Distributions of input random variables**

404   In the DBN model, the fatigue strength and traffic volume are input random variables, and the

405 correlation between joints should be considered. As a common practice [3][5][38][43], the fatigue

406 strength R is assumed to follow the lognormal distribution. According to Eurocode 3 [21], the design

407 strength at two million cycles could be considered as 100 MPa for RD joints, which is derived under

408 the 97.7% survival rate. Meanwhile, the coefficient of variation (COV) of R could be derived after the

409 COV of the material constant proposed in [44]. Through the COV, the relation between the mean and

410 standard deviation could be established, as shown in Eq.12.

$$\sigma_X = \mu_X \cdot V_X \#(12)$$

411 Where σ_X stands for the standard deviation of the variable X; μ_X and V_X are respectively mean value

412 and COV of X.

413   Basing on the above data, the mean value and standard deviation of R could be solved. The

414 detailed procedures could be referred to literature [18]. Meanwhile, the correlation coefficient could

415 be determined by Eq. 13.

$$\rho_X = 1 - \frac{V_{X,f}^2}{V_{X,p}^2} \#(13)$$

416 Where ρ_X is the mutual correlation coefficient of variable X; $V_{X,f}$ and $V_{X,p}$ are respectively the COV

417 of the entire distribution and the distribution within one deck.

418   In this study, the $V_{X,f}$ of fatigue strength is determined after the model in Eurocode 3 [21] since it

419 is established on a large-scale testing database. Meanwhile, the testing data from the article [27] are

420 used to calculate the $V_{X,p}$, in which the specimens are fabricated by the same manufacturer with the

421 steel in the same grade.

422   As aforementioned, the average daily traffic (ADT) is used to represent the traffic volume. For

423 the standard traffic model, the mean value of ADT is determined after the estimation of traffic

424 category 2 in Eurocode 1 [34], i.e. 0.5×10^6 per slow lane per year, representing the highway with a

425 medium rate of trucks.

426　　　At the same time, a COV of 0.2 is determined after the article [45] and then used to calculate the

427　standard deviation, as shown in Eq. 12. In the case of the observed model, the mean value is solved

428　after the measured data [38], while the same COV is applied to derive the standard deviation. As

429　stated before, the ADT of each joint is assumed to be perfectly correlated. Thus, the value 1.0 is used

430　for the correlation coefficient of the ADT. The input random variables are summarised in Table 5.

431

Table 5 Distribution of input random variables

Variable	Unit	Distribution	Mean	Deviation	Correlation
α_R	/1	Normal	0	1	—
α_N	/1	Normal	0	1	—
$R_{i,t}$	/MPa	Lognormal	135	19.3	0.16
$N_{i,t}$ ST[*]	/1	Normal	1631	326	1
$N_{i,t}$ OB[*]	/1	Normal	10605	2121	1

432　*: ST and OB respectively stand for the standard truck model and the observed model
433

5.2 Results and discussions

435　*5.2.1 Prediction using the standard truck and observed model*

436　　　According to codes of practice [21][39], a design life of 100 years has been considered in the

437　study. The prediction has been made using both the standard truck model and the observed model for

438　comparison purpose. Figs. 11a and b show the results of component-level reliabilities, which only

439　include the joints with initial reliability less than 8 for better illustration. According to JCSS [46],

440　targeting reliability indexes of 2.3 and 1.3 could be used for the service limit state when the costs of

441　enhancement are respectively high and low. Thus, two lines have also been used as the safety lines in

442　the comparison of component-level reliability (denoted as the upper and lower safety line for

443　distinction), below which the component is considered unreliable.

444　　　In the case of the standard truck model, only the curve of the most critical joint U12$_L$ crosses the

445　upper line after 37 years and then the lower line after 92 years. In the case of the observed model,

446　despite that the curve of U12$_L$ crosses the lines at similar times, the curve of U9$_R$ also crosses the

447　upper line after 63 years but remains above the lower line until the end of design life. Meanwhile, the

448　curves solved with the observed model are more scattered than those solved with the standard truck

449　model, since the consideration of randomness in vehicles is more comprehensive in the former model.
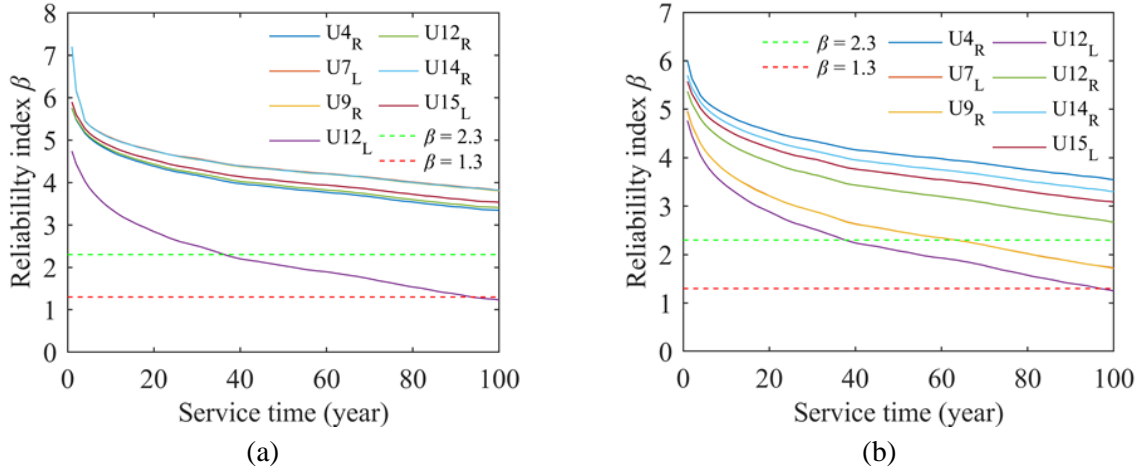
Fig. 11. Component-level reliability: (a) standard truck model; (b) observed model.

451   The system-level reliability has also been calculated using the framework established in section 3.

452   As stated before, an empirical value of failure percentage k/n = 30% is used. For comparison, analysis

453   has also been made for the situation k = 1, i.e., failure of the system occurs after the first cracking in

454   any segment. The results are shown in Figs. 12a and b. Contrary to the comparison of component-

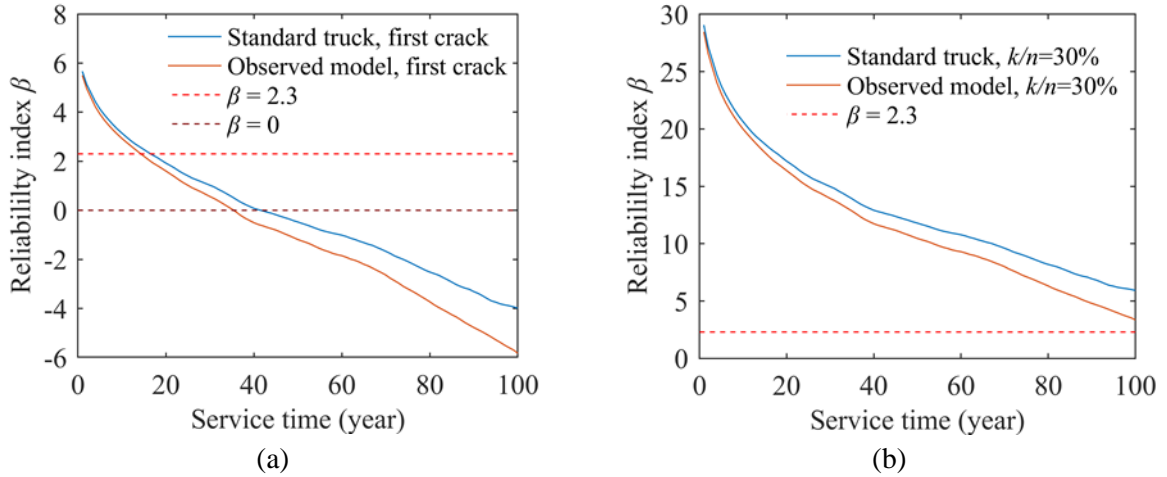455   level reliability, β = 2.3 is used as the only safety line in the comparison of system-level reliability.

456   **Fig. 12.** System-level reliability solved with two different assumptions: (a) first cracking in any

457   segment; (b) failure percentage of 30%.

458   Under both assumptions of failure, the reliability solved by the observed model is slightly lower

459   than the one solved by the standard truck at the beginning. Then, the difference in the two curves

460   increases with time and reaches its peak at the end of design life. In the case of the first cracking, the

461   two curves cross the safety line before 20 years and then gradually decrease to minus after around 40

462   years. Thus, it suggests that fatigue cracking is highly possible to occur in OSDs during the service

463   life due to the considerable number of RD joints, especially under the heavy truck traffic. In the latter

464 assumption, the lower curve solved by the observed model is still above the safety line at the end of

465 design life, illustrating that it is reliable that the proportion of failure segments will not exceed 30%.

466 Meanwhile, the observed model demonstrates the conservativeness in the system-level analysis and is

467 then employed as the default model in the following analysis if not specified.

468 *5.2.2 Enhancement of fatigue strength*

469   According to Eqs. 4 and 5, the fatigue reliability of the OSDs can be improved by enhancing the

470 fatigue strength. To achieve that, innovative details and fabrication technologies could be employed

471 [47][48]. In the study, the application of an innovative U-rib, named thickened edge U-rib (TEU), has

472 been investigated [48]. According to the test results, the strength of RD joints could be enhanced by

473 20% by using TEUs. On this basis, the analysis is made with improved strength, and the results are

474 compared in Figs. 13a and b.

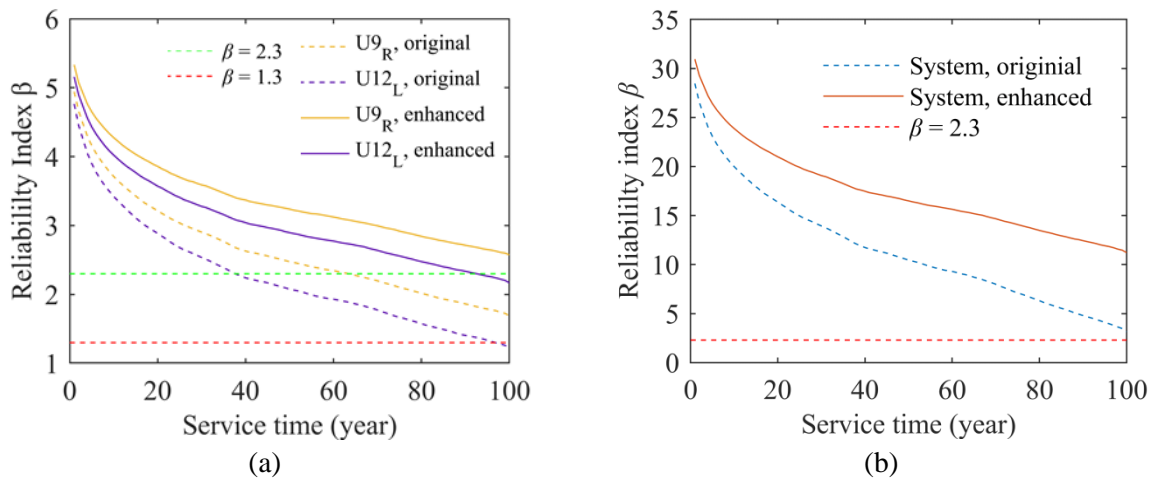(a)   (b)

475 **Fig. 13.** Reliability with and without strength enhancement: (a) component-level; (b) system-level.

476   Two critical joints, $U9_R$ and $U12_L$, are selected for the comparison of component-level reliability.

477 With the enhancement, the reliability curves move up significantly. As a result, only the reliability

478 curve of $U9_R$ becomes slightly lower than the upper safety line after almost 90 years. At the end of

479 design life, the two reliability indexes are increased by about 50%. In the case of system-level

480 reliability, at first, the difference is relatively small between the two curves, while it increases rapidly

481 with time. At the end of design life, the system-level reliability index is increased by more than 100%.

482 To summarise, a moderate enhancement in fatigue strength, i.e. 20%, could lead to significant

483 improvement in fatigue reliability at both component- and system-level. Thus, proper design and

484 fabrication are vital to the fatigue reliability of OSDs.

22

485 *5.2.3 Information-based fusion*

486   As aforementioned, the established DBN can fuse new information into the evaluation model at

487   any time when it is available. The investigation has been made on the fusion of traffic models, in

488   which the standard truck model and the observed model are used. In the analysis, the observed model

489   is assumed to be available after ten years and then fused into the model basing on the previous state.

490   The reliability index solved with information fusion is plotted against the one without information

491   fusion in Fig. 14. The result shows that after the fusion, a significant increase could be found in the

492   deterioration rate, i.e. the gradient of reliability curve. As a result, the reliability index finally reaches

493   a lower value at the end of design life. Thus, it is vital to consider the up-to-date traffic model to
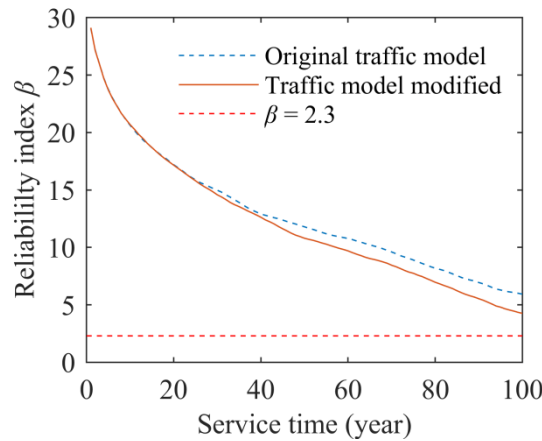
494   obtain an accurate reliability index.

495

496   **Fig. 14.** System-level reliability with the information-based fusion.

497   *5.2.4 Evidence-based updating*

498   The most important feature of the DBN lies in the capability in automatic evidence-based

499   updating, i.e., to calibrate the model using inspection results. Since the partial inspection has been

500   proved to have little effect [8], the full inspection is considered in the study, i.e., all the RD joints are

501   checked in one inspection. The deck system is assumed to be inspected three times at the 30th, 50th

502   and 70th years. Two scenes of inspection results are considered, i.e., non-detection and detection of

503   cracks.

504   The reliability index updated with the non-detection results (i.e. fatigue crack is not detected in

505   all the three inspection) has been plotted against the index without inspection in Fig. 15. The

506   reliability index is increased after each inspection since no crack is detected. Meanwhile, the

23

507 deterioration rate (i.e. the gradient of the curve) increases suddenly after the inspection and gradually

508 decreases to the normal level. It is worth noting that after the last two inspections, the reliability

509 becomes higher than the value after the first inspection. This can be attributed to the updating in the

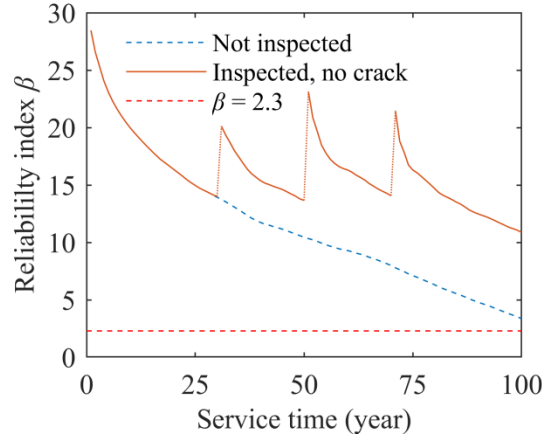510 posterior distributions of fatigue strength and ADT.

511

512 **Fig. 15.** System-level reliability with the information-based fusion.

513 The posterior distributions of the fatigue strength and ADT after inspections are derived, as

514 shown in Fig. 16a and b. The result shows that after each inspection, the distribution of strength will

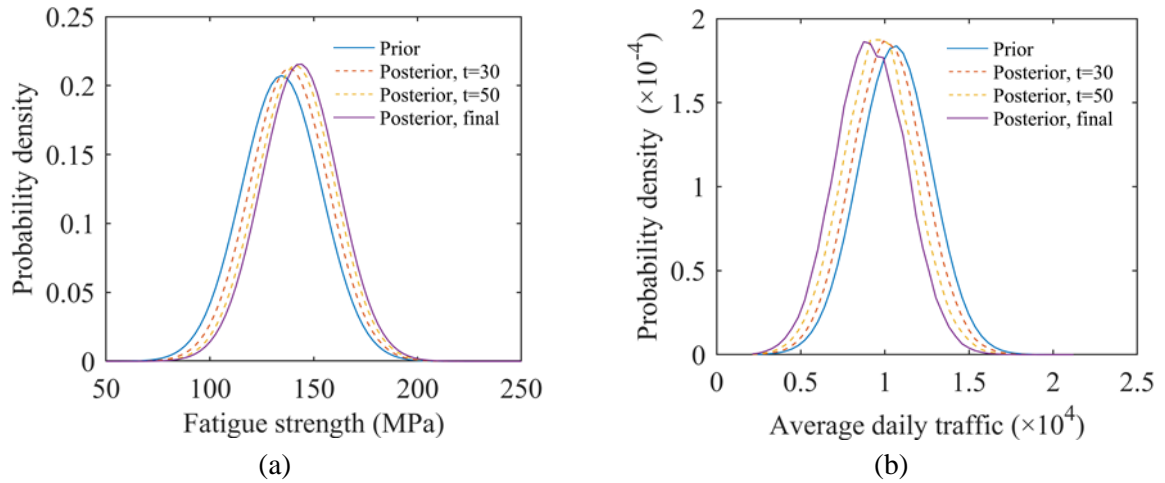515 move to the right side while that of ADT will move to the left side.

(a)   (b)

516 **Fig. 16.** Posterior distribution updated with no detection of cracks: (a) fatigue strength; (b) average

517 daily traffic (ADT).

518 Thus, the non-detection results indicate a higher value of strength and a lower value of ADT. In

519 other word, the strength is underestimated while the ADT is overestimated in the prior distributions.

520 Since the fatigue deterioration is an accumulation process, the update in posterior distribution will

521   have effects throughout the whole time slices. As a result, it can lead to a reliability index much

522   higher than the one previously predicted, as is the case in Fig. 15.

523   The situation that fatigue cracks are detected has also been analysed. The cracks are assumed to

524   be observed in different segments, to account for the most critical situation. Table 6 shows the

525   considered inspection results.

526

Table 6 Inspection results considered in the case of detection

No.	Inspection time	Number of cracked joints						
		U4$_R$	U7$_L$	U9$_R$	U12$_L$	U12$_R$	U14$_R$	U15$_L$
1	30th year	0	0	0	0	0	0	0
2	50th year	0	0	2	3	0	0	0
3	70th year	0	1	5	7	0	0	0

527

528   Based on the results, the updated reliability index can be calculated, as shown in Fig. 17. Before

529   the second inspection, the reliability is the same as the one with the non-detection results, since no

530   crack is observed until then. After the second inspection, the reliability only slightly increases since

531   crack is observed in several joints, while the deterioration rate increases significantly. After the third

532   inspection, the reliability experiences a slight increase while the deterioration rate becomes even

533   higher. As a result, the inspected curve decreases below the uninspected curve and safety line after 75

534   years and 85 years, respectively. Finally, the reliability index decreases to almost zero at the end of

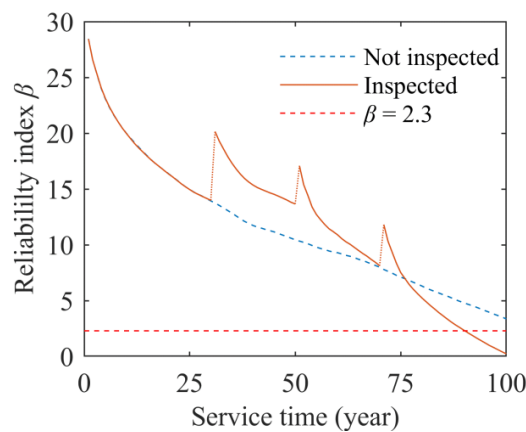535   design life.

536

537   **Fig. 17.** System-level reliability updated with the detection of cracks.

538   Similarly, the posterior distributions are also derived, as shown in Fig. 18a and b. After the first

539   inspection, the changes in the distributions are identical to the previous result with the non-detection

540   results. However, since cracks are found in the next two inspections, the distribution of strength

541   moves to the left while that of ADT moves to the right. These changes indicate the overestimation in

542   strength and the underestimation in ADT. At the same time, the change in the reliability could also be

543   explained by the updated posterior distributions: (1) the reliability increases since most of the joints

544   are not cracked when inspected; (2) the deterioration rate rises since the lower strength and high

545   traffic volume are expected.

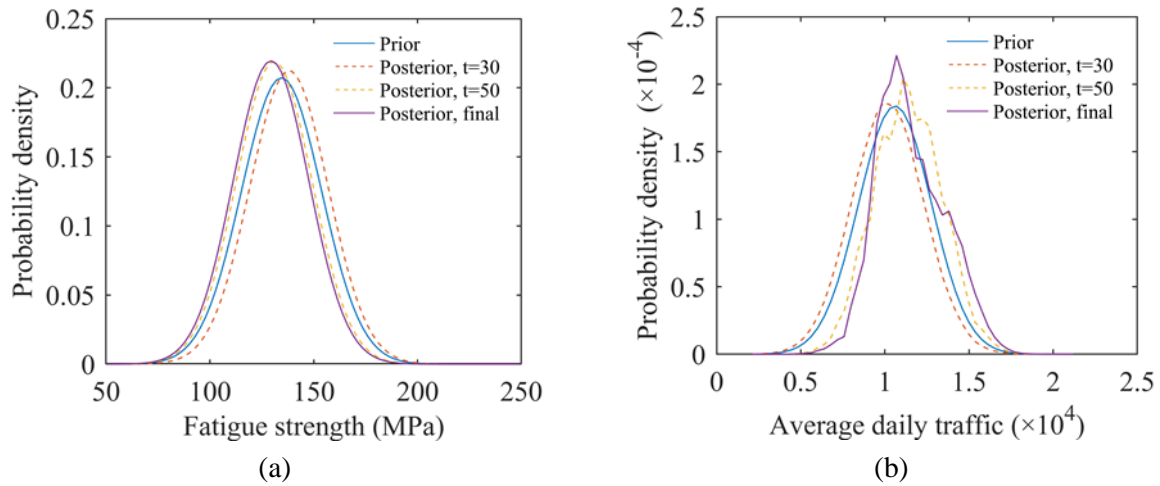(a)   (b)

546   **Fig. 18.** Posterior distribution updated with the detection of cracks: (a) fatigue strength; (b) ADT.

547   Based on the above analysis, the DBN model is capable of self-calibration through inspection

548   results. Even if the prior distributions are not well established, they could be gradually adjusted with

549   the input of inspection results. As a result, a good accuracy could be still reached for the reliability

550   prediction.

551   *5.2.5 Effects of treatment approaches*

552   After the cracking problem becomes significant, treatment approaches can be employed to

553   maintain the reliability of OSDs. Two general treatments are investigated, including maintenance and

554   traffic control. At first, maintenance is assumed to be carried out after the last inspection when the

555   cracking problem affects the safety risk after the last inspection. In the assumption, the cracked joint

556   can be fully repaired after the maintenance, i.e., recovered to the initial state. On this basis, the

557   reliability has been solved, as shown in Fig. 19. The reliability increases significantly after the

558   maintenance. At the end of design life, the reliability index is much higher than the safety line.

559   Meanwhile, the two curves are almost parallel, indicating that the maintenance has little influence on

560   the deterioration rate. This could be attributed to the following factors: (1) only the cracked joints are

26

561   manipulated through the maintenance; (2) the maintenance will not change the distributions of

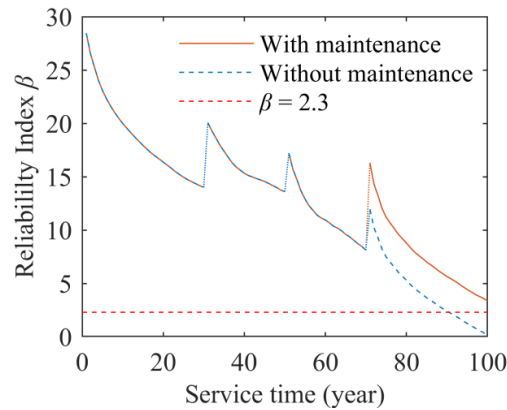562   strength and ADT, which determine the deterioration rate.

563

Fig. 19. System-level reliability with and without maintenance.

565   In the engineering practice, there are cases that maintenance cannot be carried out due to various

566   reasons such as the lack of budget, the difficulties in maintenance, the disturbance on daily traffic, and

567   so on. Alternatively, traffic control could be applied as a backup approach. Two types of controls have

568   been investigated, including the control on the vehicle weight and the control on the traffic volume.

569   At first, the average vehicle weight is assumed to be reduced by 10% due to the weight control.

570   Analysis has been made using the information-based fusion of the DBN model, as shown in Fig. 20. It

571   could be found that the deterioration rate significantly decreases after weight control. As a result, the

572   reliability curve finally reaches a value above the safety line at the end of design life.
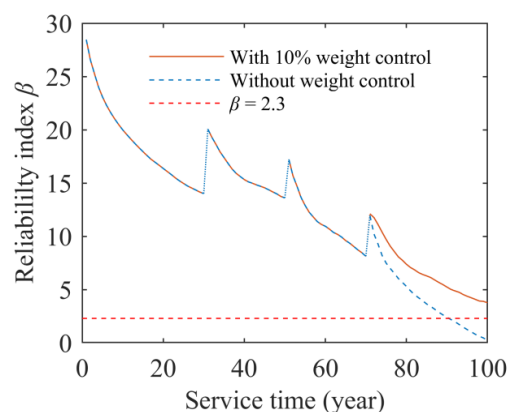
573

Fig. 20. System-level reliability with and without weight control

575   Analysis has also been made on the situation when the traffic volume is reduced by 20% due to

576   the traffic volume control, as shown in Fig. 21. A similar trend could be found, and the reliability

577   curve also reaches the value above the safety line at the end of design life.
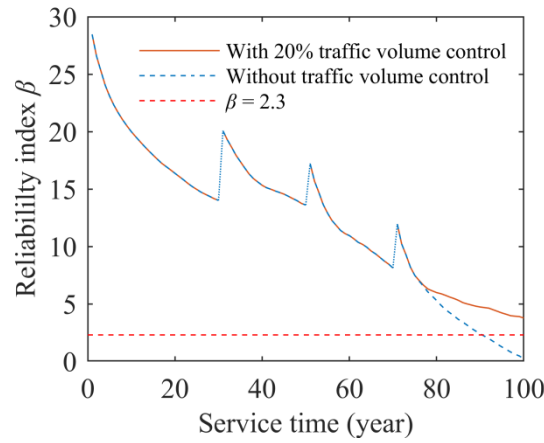
27

Fig. 21. System-level reliability with and without traffic volume control

However, traffic control should only be considered the second choice even if the reliability could be maintained at an acceptable level. To some extent, it could also be seen as a special type of degradation of serviceability, since the function of the bridge is intendedly restricted. Instead, the maintenance seems to be a suitable choice. However, as aforementioned, maintenance does not affect the uncracked joint and the deterioration rate. Thus, if the deck system is poorly designed and fabricated, extensive efforts of maintenance are required to keep the reliability at a satisfied level. Recalling the investigation on the enhancement in fatigue strength, an important conclusion could be drawn here: it is crucial to prevent the fatigue cracking by the reasonable design and elaborate fabrication, instead of the maintenance and traffic control conducted after significant cracking.

6. Concluding remarks

In this paper, a novel dynamic Bayesian network (DBN) model has been proposed for the system-level evaluation on the fatigue reliability of orthotropic steel decks (OSDs). With the model, three major tasks could be facilitated: prediction, information-based fusion, and evidence-based updating. The inference algorithm used in the model has been adapted to enable the analysis of the large-scale deck system with a considerable number of joints. After that, a system-level framework is established for the fatigue reliability of OSDs, based on the serviceability of the deck system. For illustration, a typical OSD bridge in China has been selected to carry out a case study. To derive stress spectra required by the reliability analysis, the stochastic traffic model is employed with Monte Carlo simulations. Two types of traffic models have been considered, the standard truck model and the observed model, which respectively stand for the prior and posterior knowledge about the traffic.

28

600　　Finally, the selected bridge has been investigated using the proposed approach. According to the

601　　analyses, some important conclusions could be drawn as follows:

602　　● Fatigue fracture is highly possible to occur in OSDs during the service life because a considerable

603　　　　number of welded joints are adopted, especially under the heavy truck traffic. However, OSDs

604　　　　can work with the presence of limited cracks because of their high redundancy. Thus, a

605　　　　framework of fatigue reliability at system-level is established basing on the number of cracked

606　　　　segments of OSDs, to reflect the serviceability of the deck system.

607　　● A moderate enhancement in fatigue strength of rib-to-deck joints may lead to significant

608　　　　improvement in the fatigue reliability at both the component-level and system-level. As discussed

609　　　　in the study, if the strength has been increased by 20%, the system-level reliability will be

610　　　　increased to more than two times at the end of design life, while the component-level reliability of

611　　　　two critical joints will be increased to around 150% at the end. Compared with the treatments

612　　　　such as maintenance and traffic control, special cares should be taken at the design and fabrication

613　　　　stage to improve the fatigue reliability.

614　　● Through the information fusion of the observed traffic model, it demonstrates the importance of

615　　　　considering the real-time change in the traffic model. Meanwhile, the DBN model has been

616　　　　updated with the two types of inspection results. The analysis indicates that reliability could

617　　　　change significantly with the inspection results. Thus, proper inspections should be carried out for

618　　　　OSDs, through which the prediction could be auto-calibrated.

619　　● Maintenance could be performed to maintain the reliability of OSDs after significant cracking has

620　　　　been found. After the proper maintenance, the reliability could be notably increased. However, the

621　　　　effort of maintenance has little influence on the deterioration rate, which is determined by fatigue

622　　　　strength and traffic volume. Thus, if the deck system is poorly designed and fabricated, extensive

623　　　　efforts must be made to keep its reliability at a satisfied level.

624　　● Traffic control could be applied as an alternative approach when maintenance is difficult to be

625　　　　conducted. Two types of controls have been considered, including the control on vehicle weight

626　　　　and the control on traffic volume. As a result of controls, the deterioration rate decreases, and the

627   reliability could be maintained at an acceptable level. However, traffic control should be treated

628   as a backup approach only, since the function of the bridge is intendedly restricted.

629   ● Of the most engineering concerns, the OSD can provide a 100-year service life with the proper

630   design, fabrication, inspection and maintenance during the whole lifetime.

631

639

640   **References**

641   [1]   Connor R., Fisher J., Gatti W., et al., Manual for design, construction, and maintenance of

642   orthotropic steel deck bridges, Federal Highway Administration, Washington, D.C., 2012.

643   [2]   Yang, M., Ji, B., YuanZhou, Z., & Fu, Z. (2016). Fatigue behavior and strength evaluation of

644   vertical stiffener welded joint in orthotropic steel decks, ENG. FAIL. ANAL., 70: 222-236.

645   https://doi.org/10.1016/j.engfailanal.2016.05.001

646   [3]   Kwon, K., Frangopol, D. M., & Soliman, M. (2012). Probabilistic Fatigue Life Estimation of

647   Steel Bridges by Using a Bilinear S-N Approach, J. BRIDGE ENG., 17(1): 58-70.

648   https://doi.org/10.1061/(asce)be.1943-5592.0000225

649   [4]   Pedrosa, B., Correia, J. A. F. O., Rebelo, C et al. (2019). Fatigue resistance curves for single

650   and double shear riveted joints from old Portuguese metallic bridges. ENG. FAIL. ANAL., 96:

651   255-273. https://doi.org/10.1016/j.engfailanal.2018.10.009

652   [5]   Guo, T., Frangopol, D. M., & Chen, Y. (2012). Fatigue reliability assessment of steel bridge

653   details integrating weigh-in-motion data and probabilistic finite element analysis, COMPUT.

654   STRUCT., 112-113(4): 245-257. https://doi.org/10.1016/j.compstruc.2012.09.002

655 [6] Lu, N., Noori, M., & Liu, Y. (2016). Fatigue Reliability Assessment of Welded Steel Bridge

656 Decks under Stochastic Truck Loads via Machine Learning, J. BRIDGE ENG., 22(1):

657 04016105. https://doi.org/10.1061/(asce)be.1943-5592.0000982

658 [7] Zhou, X.-Y., Treacy, M., Schmidt, F., Brühwiler, E., Toutlemonde, F., & Jacob, B. (2015).

659 Effect on Bridge Load Effects of Vehicle Transverse In-Lane Position: A Case Study, J.

660 BRIDGE ENG., 20(12): 04015020. https://doi.org/10.1061/(asce)be.1943-5592.0000763

661 [8] Maljaars, J., & Vrouwenvelder, A. C. W. M. (2014). Probabilistic fatigue life updating

662 accounting for inspections of multiple critical locations, INT. J. FATIGUE, 68(11): 24-37.

663 https://doi.org/10.1016/j.ijfatigue.2014.06.011

664 [9] Cui, C., Zhang, Q., Luo, Y., Hao, H., & Li, J. (2018). Fatigue reliability evaluation of deck-to-

665 rib welded joints in OSD considering stochastic traffic load and welding residual stress, INT. J

666 FATIGUE, 111: 151-160. https://doi.org/10.1016/j.ijfatigue.2018.02.021

667 [10] Bucher C, Computational analysis of randomness in structural mechanics: structures and

668 infrastructures book series, Vol. 3, CRC press, London, 2009.

669 https://doi.org/10.1201/9780203876534

670 [11] Lee O S, Kim D H. (2007). reliability of fatigue damaged structure using FORM, SORM and

671 fatigue mode, World Congress on Engineering 2007: 1322-1328.

672 [12] Zhao Y G, Ono T. (1999). New approximations for SORM: Part 2, J. ENG. MECH., 125(1):

673 86-93.

674 [13] Straub, D. (2009). stochastic modeling of deterioration processes through dynamic Bayesian

675 networks, J. ENG. MECH., 135(10): 1089-1099. https://doi.org/10.1061/(asce)em.1943-

676 7889.0000024

677 [14] Luque, J., & Straub, D. (2016). Reliability analysis and updating of deteriorating systems with

678 dynamic Bayesian networks, STRUCT. SAF., 62: 34-46.

679 https://doi.org/10.1016/j.strusafe.2016.03.004

680 [15] Zhu, J., Zhang, W., & Li, X. (2019). Fatigue damage assessment of orthotropic steel deck using

681 dynamic Bayesian networks, INT. J. FATIGUE, 118: 44-53.

682 https://doi.org/10.1016/j.ijfatigue.2018.08.037

683   [16]   Murphy, K. P., & B.A. (2002). Dynamic Bayesian Networks: Representation, Inference and

684   Learning. PhD Thesis, University of California, Berkeley, USA, 2002.

685   https://doi.org/10.1017/CBO9781107415324.004

686   [17]   Li, C., & Mahadevan, S. (2018). Efficient approximate inference in Bayesian networks with

687   continuous variables, RELIAB. ENG. SYST. SAFE., 169: 269-280.

688   https://doi.org/10.1016/j.ress.2017.08.017

689   [18]   Hobbacher A., Recommendations for fatigue design of welded joints and components, second

690   ed., Springer, Switzerland, 2016. https://doi.org/10.1007/978-3-319-23757-2

691   [19]   Marques, F., Correia, J. A. F. O., de Jesus, A. M. P., et al. (2018). Fatigue analysis of a railway

692   bridge based on fracture mechanics and local modelling of riveted connections. ENG. FAIL.

693   ANAL., 94: 121-144. https://doi.org/10.1016/j.engfailanal.2018.07.016

694   [20]   Niemi E, Fricke W, Maddox S J., Fatigue analysis of welded components: designer's guide to

695   the structural hot-spot stress approach, Woodhead publishing, Cambridge, 2006.

696   https://doi.org/10.1201/9781439824016

697   [21]   European committee for standardization, EN 1993: Eurocode 3 – design of steel structures,

698   CEN, Brussels, 2005.

699   [22]   Baptista, C., Reis, A., & Nussbaumer, A. (2017). Probabilistic S-N curves for constant and

700   variable amplitude, INT. J. FATIGUE, 101: 312-327.

701   https://doi.org/10.1016/j.ijfatigue.2017.01.022

702   [23]   Devore J. L., Probability and statistics for engineering and the sciences, Cengage learning,

703   Boston, 2011. https://doi.org/10.2307/2532427

704   [24]   Liu, P. L., & Der Kiureghian, A. (1986). Multivariate distribution models with prescribed

705   marginals and covariances, PROBABILIST. ENG. MECH., 1(2): 105-112.

706   https://doi.org/10.1016/0266-8920(86)90033-0

707   [25]   Korb K. B., Nicholson A. E., Bayesian artificial intelligence, second ed., CRC press, London,

708   2010. https://doi.org/10.1111/j.1751-5823.2011.00159_18.x

709   [26]   Schneider, R., Thöns, S., & Straub, D. (2017). Reliability analysis and updating of deteriorating

710   systems with subset simulation, STRUCT. SAF., 64: 20-36.

711   https://doi.org/10.1016/j.strusafe.2016.09.002

712   [27]   Heng, J., Zheng, K., Gou, C., Zhang, Y., & Bao, Y. (2017). Fatigue performance of rib-to-deck

713   joints in orthotropic steel decks with thickened edge u-ribs, J. BRIDGE ENG., 22(9):

714   04017059. https://doi.org/10.1061/(asce)be.1943-5592.0001095

715   [28]   Fisher, J. W., & Barsom, J. M. (2015). Evaluation of cracking in the rib-to-deck welds of the

716   Bronx–Whitestone bridge, J. BRIDGE ENG., 21(3): 04015065.

717   https://doi.org/10.1061/(asce)be.1943-5592.0000823

718   [29]   Gollwitzer, S., & Rackwitz, R. (1990). On the reliability of Daniels systems, STRUCT. SAF.,

719   7(2-4): 229-243. https://doi.org/10.1016/0167-4730(90)90072-W

720   [30]   Fisher, J. W., & Roy, S. (2011). Fatigue of steel bridge infrastructure, STRUCT.

721   INFRASTRUCT E., 7(7):457-475. https://doi.org/10.1080/15732479.2010.493304

722   [31]   Leander, J., Honfi, D., Larsson Ivanov, O., & Björnsson, Í. (2018). A decision support

723   framework for fatigue assessment of steel bridges, ENG. FAIL. ANAL., 91: 306-314.

724   https://doi.org/10.1016/j.engfailanal.2018.04.033

725   [32]   Ngamkhanong, C., Kaewunruen, S., & Costa, B. (2018). State-of-the-art review of railway

726   track resilience monitoring, Infrastructures, 3(1): 3.

727   https://doi.org/10.3390/infrastructures3010003

728   [33]   AASHTO, AASHTO LRFD bridge design specifications, sixth ed., Washington, D.C., 2012.

729   [34]   European committee for standardization, EN 1991-2:2003 Eurocode 1: Actions on structures–

730   part 2: traffic loads on bridges, CEN, Brussels, 2003.

731   [35]   Kaewunruen S., & Remennikov A. M. (2009). Structural safety of railway prestressed concrete

732   sleepers, AUS. J. STRUCT. ENG., 9(2): 129-140.

733   https://doi.org/10.1080/13287982.2009.11465016

734   [36]   Dindar, S., Kaewunruen, S., An, M., & Sussman, J. M. (2018). Bayesian network-based

735   probability analysis of train derailments caused by various extreme weather patterns on railway

736   turnouts, SAFETY SCI., 110: 20-30. https://doi.org/10.1016/j.ssci.2017.12.028

737 [37] Liu, Y., Zhang, H., Liu, Y., Deng, Y., Jiang, N., & Lu, N. (2017). Fatigue reliability assessment

738   for orthotropic steel deck details under traffic flow and temperature loading, ENG. FAIL.

739   ANAL., 71: 179-194. https://doi.org/10.1016/j.engfailanal.2016.11.007

740 [38] Guo, T., Liu, Z., Pan, S., & Pan, Z. (2015). Cracking of longitudinal diaphragms in long-span

741   cable-stayed bridges, J. BRIDGE ENG., 20(11): 04015011.

742   https://doi.org/10.1061/(asce)be.1943-5592.0000771

743 [39] Ministry of communications of the People's Republic of China. Specifications for design of

744   highway steel bridges (GB/T D64-2015), CCPress, Beijing, 2015 (in Chinese).

745 [40] ANSYS Inc. ANSYS software. Canonsburg, PA, USA. https://www.ansys.com/

746 [41] MathWorks Inc. MATLAB software. Natick, MA, USA. https://www.mathworks.com/

747 [42] Amzallag, C., Gerey, J. P., Robert, J. L., & Bahuaud, J. (1994). Standardization of the rainflow

748   counting method for fatigue analysis, INT. J. FATIGUE, 16(4): 287-293.

749   https://doi.org/10.1016/0142-1123(94)90343-3

750 [43] Shen. The statistical analysis of fatigue data, PhD Thesis, University of Arizona, Tucson, 1994.

751 [44] Zhao, Z., Haldar, A., & Breen, F. L. (2006). Fatigue reliability evaluation of steel bridges, J.

752   STRUCT. ENG., 120(5): 1608-1623. https://doi.org/10.1061/(asce)0733-

753   9445(1994)120:5(1608)

754 [45] Lu, N., Liu, Y., & Deng, Y. (2019). Fatigue reliability evaluation of orthotropic steel bridge

755   decks based on site-specific weigh-in-motion measurements, INT. J. STEEL STRUCT., 19(1):

756   181-192. https://doi.org/10.1007/s13296-018-0109-8

757 [46] JCSS probabilistic model code, part 1: basis of design, JCCS, Aalborg, 2000.

758 [47] Zhang, Q., Liu, Y., Bao, Y., Jia, D., Bu, Y., & Li, Q. (2017). Fatigue performance of

759   orthotropic steel-concrete composite deck with large-size longitudinal U-shaped ribs, ENG.

760   STRUCT., 150: 864-874. https://doi.org/10.1016/j.engstruct.2017.07.094

761 [48] Heng, J., Zheng, K., Zhang, Y., & Wang, Y. (2018). Enhancing fatigue performance of rib-to-

762   deck joints in orthotropic steel decks using thickened edge U-ribs, Structures Congress 2018:

763   359-369. https://doi.org/10.1061/(ASCE)BE.1943-5592.0001095.